The Astrophysical Journal, 585:899–907, 2003 March 10

CONTINUED RADIO MONITORING OF THE GAMMA-RAY BURST 991208

T. J. Galama,[1] D. A. Frail,[2] R. Sari,[3] E. Berger,[1] G. B. Taylor,[2] and S. R. Kulkarni[1]

Received 2002 October 3; accepted 2002 November 12

ABSTRACT

We present radio observations of the afterglow of the bright γ-ray burst GRB 991208 at frequencies of 1.4, 4.9, and 8.5 GHz, taken between two weeks and 300 days after the burst. The well-sampled radio light curve at 8.5 GHz shows that the flux density peaked about 10 days after the burst and decayed thereafter as a power law $F_R \propto t^{-1.07\pm0.09}$. This decay rate is more shallow than the optical afterglow of GRB 991208 with $F_0 \propto t^{-2.2}$, which was measured during the first week. These late-time data are combined with extensive optical, millimeter, and centimeter measurements and fitted to the standard relativistic blast wave model. In agreement with previous findings, we find that an isotropic explosion in a constant-density or wind-blown medium cannot explain these broadband data without modifying the assumption of a single power-law slope for the electron energy distribution. A jetlike expansion provides a reasonable fit to the data. In this case, the flatter radio light curve compared to the optical may be due to emission from an underlying host galaxy, or due to the blast wave making a transition to nonrelativistic expansion. The model that best represents the data is a free-form model in which it is assumed that the broadband emission originates from a synchrotron spectrum, while the time evolution of the break frequencies and peak flux density are solved for explicitly. Although the decay indices for most of the synchrotron parameters are similar to those for the jet model, the evolution of the cooling break is unusually rapid ($\nu_c \propto t^{-2}$) and therefore requires some nonstandard evolution in the shock.

Subject headings: cosmology: observations — gamma rays: bursts — radio continuum: general

1. INTRODUCTION

The afterglow of GRB 991208 was one of the brightest observed to date. Shortly after the coordinates of the γ-ray error box were made known, a previously uncataloged radio source was discovered near its center. Based on the source location, its inverted spectrum, and compactness, it was a strong candidate for being the radio counterpart of GRB 991208 (Frail et al. 1999). This was confirmed by the subsequent discovery of an optical transient at the same location as the radio source (Castro-Tirado et al. 1999). Follow-up optical observations taken from 2 to 7 days after the burst showed that the spectral and temporal characteristics of this burst could be represented by power-law indices $\alpha = 2.2 \pm 0.1$ and $\beta = 0.75 \pm 0.03$, where $F(t) \propto t^{-\alpha}\nu^{-\beta}$ (Sagar et al. 2000). With added data, Castro-Tirado et al. (2001) determined an $\alpha = 2.3 \pm 0.07$ and a somewhat steeper $\beta = 1.05 \pm 0.09$. The γ-ray properties, the localization, and the subsequent afterglow discovery for GRB 991208 are presented in more detail by Hurley et al. (2000).

GRB 991208 was also very bright at millimeter wavelengths (Shepherd et al. 1999), and as a consequence, well-sampled spectra and light curves covering frequencies between 1.43 and 240 GHz were taken during the initial two weeks following the burst (Galama et al. 2000, hereafter Paper I). These observations made it possible, for the first time, to trace the time evolution of the synchrotron spectrum directly without resorting to specific models for the evolution of the characteristic frequencies and the peak flux density. In comparing these results with model predictions, it was found that spherically symmetric explosions in homogeneous or wind-blown circumburst media could be ruled out. A model in which the relativistic outflow is collimated (i.e., a jet) was shown to account for the observed evolution of the synchrotron parameters, the rapid decay at optical wavelengths, and the observed radio to optical spectral flux distributions, provided that the jet transition has not been fully completed in the first two weeks after the event.

This high quality data set stimulated other modeling efforts for GRB 991208. Li & Chevalier (2001) argued that an isotropic explosion in a wind-blown ambient medium described the data equally well. However, in order to account for the fast decay of the optical light curves with respect to the radio light curves, they invoked a nonstandard break in the electron energy distribution. Panaitescu & Kumar (2002) also required a broken power law and they concluded that the best fit to the data was obtained for a jetlike outflow with an opening angle of about 15° expanding into either a constant density or wind-blown circumburst medium. Dai & Gou (2001) present a variation on these other efforts, arguing that the steep optical decay is due to an anisotropic jet viewed off-axis, which is expanding into a wind from a red supergiant.

In view of the disparate conclusions reached on the basis of this early afterglow data, there is some hope that with further monitoring of the afterglow it may be possible to distinguish between these models. Accordingly, in this paper we present radio observations of GRB 991208 made with the VLA and the Very Large Baseline Array (VLBA), which began at the end of the two week period covered in Paper I and continued until the burst faded below our detection limits. We focus on the interpretation of the observations in terms of the predictions made by relativistic blast wave models. The observations and results are presented in § 2 and § 3 and are discussed in § 4.

[1] Division of Physics, Mathematics and Astronomy, California Institute of Technology, MS 105-24, Pasadena, CA 91125.

[2] National Radio Astronomy Observatory, P.O. Box 0, Socorro, NM 87801.

[3] California Institute of Technology, Theoretical Astrophysics 103-33, Pasadena, CA 91125.

2. OBSERVATIONS

2.1. *Very Large Array*

Observations at 1.43, 4.86, and 8.46 GHz were made using the NRAO Very Large Array (VLA).[4] All observations were performed in the default continuum mode in which, at each frequency, the full 100 MHz bandwidth was used in two adjacent 50 MHz bands. The synthesized beam at 8.46 GHz was approximately 0.″8. The beam size at other frequencies scales inversely with frequency. Gain calibration was carried out by observing 3C 48. The array phase was monitored by switching between the GRB and the phase calibrators J1637+462 (at 8.46 GHz), J1658+476 (at 4.86 GHz), and J1653+397 (at 1.43 GHz). Data calibration and imaging were carried out with the AIPS software package following standard practice. We performed phase self-calibration on the 1.43 GHz data. Flux densities were determined by a least-squares fitting of the Gaussian-shaped synthesized beam to the source. For very faint detection levels ($<3\,\sigma$), we used the peak flux density at the position of the radio counterpart (Frail et al. 1999). A log of the observations is provided in Table 1.

[4] The NRAO is a facility of the National Science Foundation operated under cooperative agreement by Associated Universities, Inc.

2.2. *Very Long Baseline Array*

Observations centered at 8.35 and 4.85 GHz were made using the NRAO Very Long Baseline Array (VLBA) at four epochs. At both frequencies the observations consisted of eight channels of bandwidth 8 MHz (64 MHz total bandwidth) spaced equally over a $\sim$0.5 GHz frequency span. The phases were calibrated using the calibrator source 1637+472. At each epoch the observations lasted $\sim$9 hr (divided over the source, calibrators, and frequency switches). These observations were designed for an interstellar scintillation experiment (requiring substantial time and frequency span), the results of which will be presented in a separate paper. In Table 2 we report just the time-averaged flux densities.

TABLE 1
SUMMARY OF VLA OBSERVATIONS OF GRB 991208

Date (UT)	t_{start}–t_{end} (hh:mm:ss)	t_{int} (hh:mm:ss)	Δt (days)	$F_{8.46}$ (μJy)	$F_{4.86}$ (μJy)	$F_{1.43}$ (μJy)
1999 Dec 23.80	19:03:30–19:17:30	11:20	15.61	782 ± 40		
1999 Dec 26.78	18:25:40–18:47:20	16:20	18.59	693 ± 38		
1999 Dec 28.98	23:14:50–23:38:10	35:30	20.79	464 ± 44		
1999 Dec 29.49	11:17:10–12:11:50	22:00	21.30	679 ± 30		
1999 Dec 29.49	11:17:10–12:11:50	18:40	21.30		501 ± 42	
1999 Dec 29.49	11:29:20–12:41:17	36:20	21.30			79 ± 41
2000 Jan 5.94	22:25:00–22:37:10	9:30	28.75	646 ± 58		
2000 Jan 9.89	21:04:50–21:48:00	19:00	32.70	337 ± 34		
2000 Jan 9.89	20:58:00–21:37:50	14:25	32.70			61 ± 53
2000 Jan 13.79	18:13:10–19:33:00	31:30	36.60	574 ± 25		
2000 Jan 13.79	18:04:55–19:41:05	30:35	36.60			56 ± 40
2000 Jan 17.85	19:33:40–21:17:30	43:30	40.66	400 ± 23		
2000 Jan 17.85	19:29:40–21:00:10	26:30	40.66			73 ± 42
2000 Jan 21.92	21:17:30–22:36:20	31:40	44.73	458 ± 31		
2000 Jan 21.92	21:11:50–22:43:50	28:30	44.73			98 ± 59
2000 Jan 24.81	19:03:25–19:52:00	36:50	47.62		212 ± 29	
2000 Jan 25.85	18:32:10–22:25:20	1:00:10	48.66	442 ± 23		
2000 Jan 25.85	18:28:00–22:19:40	1:02:55	48.66			54 ± 37
2000 Jan 30.85	18:42:30–22:22:30	1:20:50	53.66	290 ± 21		
2000 Jan 30.85	18:38:10–22:13:20	1:02:55	53.66			43 ± 41
2000 Feb 4.80	18:22:50–19:59:20	38:00	58.61	239 ± 24		
2000 Feb 4.80	18:18:30–20:06:30	31:45	58.61			82 ± 43
2000 Feb 10.78	17:59:10–19:18:00	31:30	64.59	232 ± 27		
2000 Feb 10.78	17:55:00–19:26:40	26:55	64.59			60 ± 49
2000 Mar 13.63	14:42:50–15:37:20	40:50	96.44	172 ± 33		
2000 Mar 27.57	13:34:20–13:48:50	11:50	110.38	177 ± 47		
2000 Apr 13.67	15:43:50–16:36:20	38:50	127.48	123 ± 26		
2000 May 4.62	14:27:40–16:20:50	2:01:10	148.43	106 ± 23		
2000 May 7.64	14:30:50–16:24:50	1:24:20	151.45	152 ± 25		
2000 Jun 6.45	10:31:10–11:09:30	24:40	181.26	38 ± 40		
2000 Jun 14.40	09:24:10–10:01:10	27:00	189.21	29 ± 30		
2000 Aug 27.76	22:15:30–23:08:10	42:00	263.57	31 ± 27		
2000 Sep 10.85	20:28:10–21:19:10	01:25:20	277.66	44 ± 21		
2000 Sep 16.78	18:37:00–21:25:30	02:28:50	283.59	20 ± 19		
2000 Sep 24.77	18:35:30–20:53:40	02:02:03	291.58	51 ± 15		
2000 Sep 27.10	02:19:10–03:40:30	01:05:30	293.91			

NOTES.—The date, start time t_{start}, and end time t_{end} of the observations are given in UT. Also, the total time on source t_{int}, the time passed since the event Δt and the fluxes at 8.46, 4.86, and 1.43 GHz are given. Observations taken before 1999 December 22 can be found in Paper I.

TABLE 2
SUMMARY OF VLBA OBSERVATIONS OF GRB 991208: THE DATE, THE TIME PASSED SINCE THE EVENT Δt, AND THE FLUXES AT 8.35 AND 4.85 GHz

Date (UT)	Δt (days)	$F_{8.35}$ (μJy)	$F_{4.85}$ (μJy)
1999 Dec 14.73.....	6.54	967 ± 55	448 ± 67
1999 Dec 18.72.....	10.53	1008 ± 60	888 ± 74
1999 Dec 26.70.....	18.51	430 ± 75	431 ± 92
1999 Jan 4.69.....	27.50	474 ± 56	440 ± 64

3. RESULTS

Multiwavelength light curves of the event are presented in Figure 1. Data are from this work (Tables 1 and 2) and Paper I. Optical observations are taken from Castro-Tirado et al. (2001), where we have only included early data (less than 10 days after the event) to measure the "pure" afterglow emission (i.e., where the underlying host does not contribute significantly).

The VLBA measurements may suffer from amplitude losses as a result of imperfect phase referencing. The light curves indicate that such losses may be significant, since at 8.46 GHz the VLBA data seem to be systematically lower than the VLA data.

The 8.46 and 4.86 GHz light curves rise to a maximum at around 10 days. While the 8.46 GHz light curve is smoothly rising to a maximum of about 2 mJy during the first week, it undergoes a sudden drop to about 1 mJy (around 9 days after the burst) followed by a second peak (at around 12 days). Such erratic flux density variations are the hallmark of interstellar scintillation. We will return to this point in § 3.1. The overall trend in Figure 1 is for the peak flux density to decline with decreasing frequency. A linear least-squares fit was carried out to the late-time radio light curve ($\Delta t = 53$–293 days) at 8.46 GHz, and we derived a temporal decay index $\alpha_R = 1.07 \pm 0.09$ ($\chi^2_r = 1.07$, where $F_R \propto t^{-\alpha_R}$). This is to be compared with the much steeper optical decay $\alpha_o = 2.2 \pm 0.1$ determined at $\Delta t = 2$–10 days (Sagar et al. 2000). Reconciling this difference between the optical and radio decay indices is one of the main challenges in modeling the afterglow of GRB 991208 (see § 4).

3.1. *Interstellar Scintillation*

The lines of sight toward most GRBs traverse a considerable path length through the turbulent ionized gas of our Galaxy. As a result, the radio emission from GRB afterglows is expected to be affected by interstellar scattering (ISS). Indeed, as predicted by Goodman (1997), ISS has been positively identified in several cases (e.g., Frail et al. 1997). The subject of ISS is a large one (see review by Rickett 1990) and encompasses a range of observational phenomenology. Here we concern ourselves with estimating the importance of ISS-induced modulation of our flux density measurements as a function of time and frequency. For more detailed treatments of ISS see Goodman (1997) and Walker (1998).

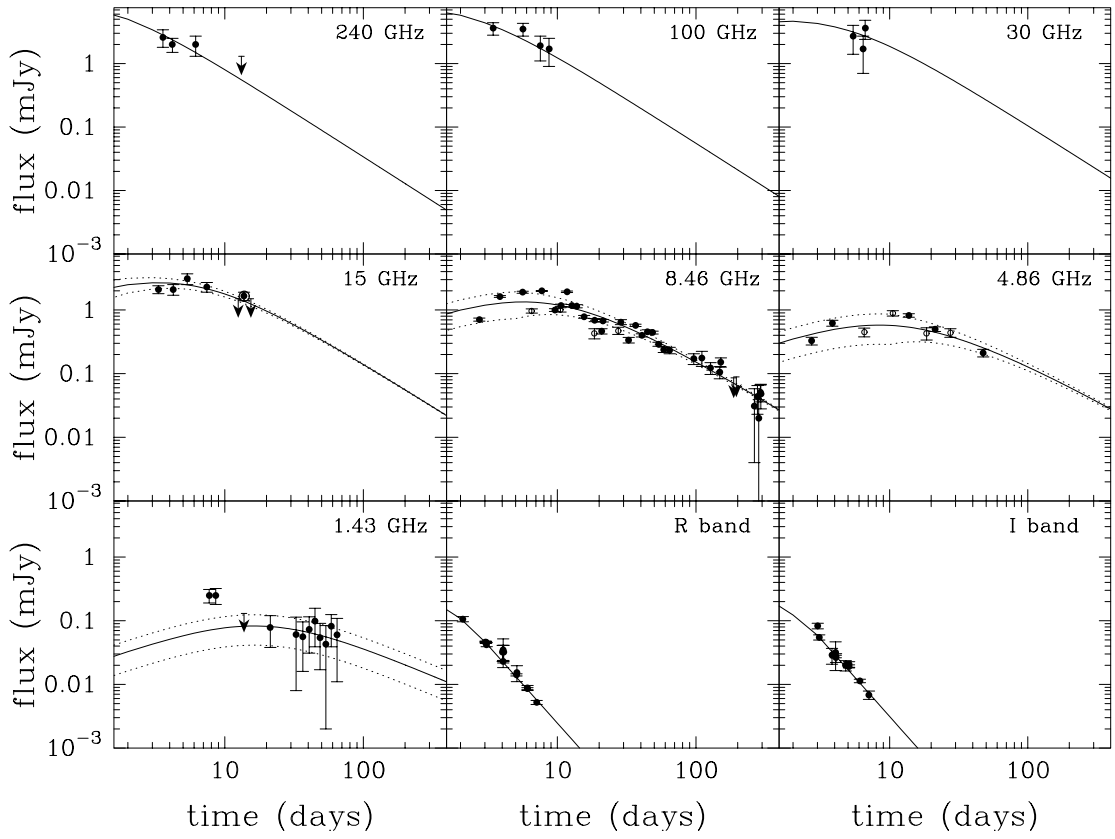

FIG. 1.—Radio to optical light curves of GRB 991208. Data are from this work (Table 1) and Paper I. Optical observations are from Castro-Tirado et al. (2001). Open symbols indicate the VLBA data (Table 2). The solid line indicates the best free-form fit to the light curves, and the dotted lines are the predicted rms scatter due to interstellar scintillation. See § 3 for more details.

The character of the expected flux density fluctuations depend on whether the scattering takes place in the "strong" or "weak" regimes. We define a transition frequency ν_0, below which the density irregularities can induce strong phase variations and above which there is only weak scattering (WISS). Strong scattering can result in both slow, broadband changes, due to refractive interstellar scintillation (RISS), and fast, narrowband variations due to diffractive interstellar scintillation (DISS). The value of ν_0 along any given line of sight depends on the strength of the scattering and the total path length. The amount of scattering is parameterized by the scattering measure, SM, as modeled for the Galaxy by Taylor & Cordes (1993). For convenience we assume that the scattering along the line of sight takes place in a thin screen located at $d_{\rm scr} \sim (h_z/2)\ \sin|b|^{-1}$, where h_z ($\simeq$1 kpc) is the exponential scale height of the ionized gas layer (Reynolds 1989).

Radio afterglow emission will be modulated by ISS provided that the source size θ_s is close to one of the three characteristic angular scales (1) $\theta_w = \theta_{F_0}(\nu_0/\nu)^{1/2}$, (2) $\theta_d = \theta_{F_0}(\nu_0/\nu)^{-6/5}$, or (3) $\theta_r = \theta_{F_0}(\nu_0/\nu)^{11/5}$, where θ_{F_0} is the angle subtended by the first Fresnel zone at the scattering screen for $\nu = \nu_0$, i.e., $\theta_{F_0} = (c/2\pi\nu_0 d_{\rm scr})^{1/2}$. The modulation index m_p (i.e., the rms fractional flux variation) is given by

$$m_p = \begin{cases} (\nu_0/\nu)^{17/12} & \text{for } \nu > \nu_0 \text{ and } \theta_s < \theta_w \text{ (WISS)}, \\ 1 & \text{for } \nu < \nu_0 \text{ and } \theta_s < \theta_d \text{ (DISS)}, \\ (\nu_0/\nu)^{-17/30} & \text{for } \nu < \nu_0 \text{ and } \theta_s < \theta_r \text{ (RISS)}. \end{cases} \quad (1)$$

The expansion of the afterglow may cause θ_s to eventually exceed one or more of the three characteristic angular scales that define the different scattering regimes. For ease of comparison in the Appendix we compute θ_s for three different interstellar medium (ISM) models (a constant density ISM model, a wind model [WIND], and a jet model [JET]; see § 3.2). Then the modulation will begin to "quench" as follows:

$$m_\nu = m_p \times \begin{cases} (\theta_w/\theta_s)^{7/6} & \text{for } \nu > \nu_0 \text{ and } \theta_s > \theta_w \text{ (WISS)}, \\ (\theta_d/\theta_s) & \text{for } \nu < \nu_0 \text{ and } \theta_s > \theta_d \text{ (DISS)}, \\ (\theta_r/\theta_s)^{7/6} & \text{for } \nu < \nu_0 \text{ and } \theta_s > \theta_r \text{ (RISS)}. \end{cases} \quad (2)$$

For GRB 991208 at $(l,\ b) = (72\overset{\circ}{.}4,\ +42\overset{\circ}{.}6)$ we estimate SM $= 2.26 \times 10^{-4}$ kpc m$^{-20/3}$ from the Taylor & Cordes (1993) model. Taking a typical scattering screen distance of $d_{\rm scr} = 0.74$ kpc we compute $\nu_0 = 4.8$ GHz and $\theta_{F_0} = 4.2$ μas (Walker 1998). The difficulties in obtaining accurate estimates of SM and $d_{\rm scr}$ likely limit the accuracy of the ν_0 and θ_{F_0} values to $\pm$30%. In Figure 2 we plot these values along with lines showing the different ISS regimes. On the right-hand side of the figure we compute a model-dependent timescale for the fireball to reach the angular size given on the left-hand side. We have assumed that the emission from GRB 991208 originates from a jetlike outflow for $t_{\rm jet} \leq 2$ days and used the relevant expression for θ_s in the Appendix. At a redshift $z = 0.7055$ (Dodonov et al. 1999; Djorgovski et al. 1999) the angular distance $D_A = D_L/(1+z)^2 = 0.45 \times 10^{28}$ cm, where D_L is the luminosity distance. The source size is $\theta_s = 5.2(E_{52}/n_1)^{1/8}(t_d/15)^{1/2}$ μas,

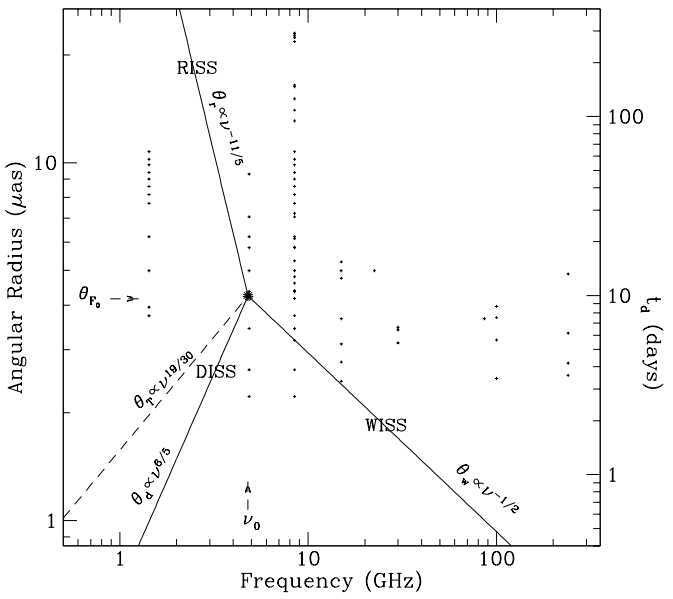

FIG. 2.—Interstellar scattering toward GRB 991208 with the three regimes of scattering: weak (WISS), diffractive (DISS), and refractive (RISS). The solid lines indicate the frequency dependence of each of three characteristic angular scales, joined at the transition frequency ν_0 and the Fresnel scale θ_{F_0}. On the right vertical axis we compute a model-dependent timescale, corresponding to the angular radius reached by a collimated fireball given on the left vertical axis. The small crosses indicate the time and frequency of the measurements in Tables 1 and 2. See § 3 for more details.

where E_{52} is the energy in the blast wave in units of 10^{52} ergs and n_1 is the density of the ambient medium in particles cm^{-3}. Thus, the observations in Tables 1 and 2 (and indicated as small crosses in Fig. 2) lie on either side of ν_0 and were taken during a time when θ_s expanded to eventually exceed θ_{F_0}.

It is apparent in Figure 2 that most of the observations were taken in the weak scattering regime ($\nu > \nu_0$). Furthermore, for $\nu > 15$ GHz, $\theta_s > \theta_w$ and therefore we expect that the observed variations will be dominated by source evolution and measurement error, not ISS. ISS starts to become comparable to the measurement error at 15 GHz, where it is straightforward to show that $m_{15} = 0.08(t_d/15)^{-7/12}$ (for $\theta_s \geq \theta_w$).

Accounting for ISS is particularly important at 8.46 GHz since the measurement error at this frequency is small (<5%) while we expect $m_{8.46} = 0.45$ for $\theta_s < \theta_w$ and for $t_d \gtrsim 5$ days $m_{8.46} = 0.24(t_d/15)^{-7/12}$. Since the 8.46 GHz light curve is so well sampled, we can independently check on this prediction by subtracting out any linear trend and computing the scatter. For different assumed curves we find within the first two weeks of observations an rms scatter of 20%–30%, suggesting that the strength of scattering along this line of sight may be slightly weaker than we have predicted.

We also expect large variations in the flux density at $\nu = 4.86$ GHz, but these are difficult to quantify, owning to the proximity of ν_0 (Walker 1998). For the purposes of model fitting we adopt $m_{4.86} = 0.5$ and for $t_d \gtrsim 10$ days $m_{4.86} = 0.40(t_d/15)^{-7/12}$.

The line $\theta_T = \theta_{F_0}(\nu_0/\nu)^{-19/30}$ indicates the transition diameter that separates the region where the modulations are RISS dominated (above θ_T) from that where they are DISS dominated (below θ_T). The observations at

$\nu = 1.43$ GHz are clearly in the strong regime ($\nu < \nu_0$) where $\theta_d < \theta_s < \theta_r$, and where RISS is expected to be significant with $m_p = 0.5$ on refractive timescales of a day or more. Shorter timescale ($t_{\rm DISS} \sim 3$ hr) variations due to DISS are also expected but at a reduced level of 10%–15%, suppressed by the finite source size (i.e., $\theta_s \gg \theta_d$) and bandwidth averaging. DISS, unlike WISS and RISS, is a *narrowband* phenomenon with a decorrelation bandwidth $\Delta\nu_d = \nu(\nu/\nu_0)^{17/5} <$ 100 MHz, the bandwidth of our observations.

3.2. *Synchrotron Emission*

The radio/mm/optical to X-ray afterglow emission is believed to arise from the forward shock of a relativistic blast wave that propagates into the circumburst medium (see Piran 2000 and van Paradijs, Kouveliotou, & Wijers 2000 for reviews). The electrons are assumed to be accelerated to a power-law distribution in energy, $dN/d\gamma_e \propto \gamma_e^{-p}$, for $\gamma > \gamma_m$, and to radiate synchrotron emission; where γ_e is the Lorentz factor of the electrons, γ_m is the minimum Lorentz factor, and p is the power-law index of the electron energy distribution. Detailed calculations by Granot, Piran, & Sari (1999a, 1999b) and Granot & Sari (2002) have shown that to good approximation (to within a few percent) the synchrotron afterglow spectrum can be described by the following function:

$$F(\nu, F_m, \nu_a, \nu_m, p) = F_m\,(2)^{-1/n}\left\{1 - \exp\left[-(\nu/\nu_a)^{-5/3}\right]\right\}\left(\frac{\nu}{\nu_a}\right)^{5/3} \times \left[\left(\frac{\nu}{\nu_m}\right)^{n/3} + \left(\frac{\nu}{\nu_m}\right)^{-(p-1)n/2}\right]^{1/n}, \quad (3)$$

where F_m is the synchrotron peak flux density at the peak frequency ν_m, and ν_a is the synchrotron self-absorption frequency. The index $n = -0.837$ (Granot & Sari 2002) and controls the sharpness of the peak at ν_m. We have assumed slow cooling, i.e., $\nu_m \ll \nu_c$, where ν_c is the synchrotron cooling frequency. Castro-Tirado et al. (2001) have measured a steeper optical slope β than Sagar et al. (2000) and have argued that this is evidence that the afterglow observations of GRB 991208 require the synchrotron cooling break to be located between radio and optical wavelengths. We model a possible synchrotron cooling break by a sharp spectral break with decrement $\Delta\beta = 0.5$ at $\nu = \nu_c$, and parameterization $\nu_c = C_c t^{-\alpha_c}$.

The evolution of the break frequencies ν_a and ν_m, the cooling frequency ν_c, and the peak flux density F_m follows from assumptions on the dynamics of the relativistic blast wave. It is common practice to assume three cases: (i) propagation into a constant density ambient medium (ISM; Sari, Piran, & Narayan 1998), (ii) propagation into a wind-stratified ambient medium (WIND; Chevalier & Li 1999, 2000), and (iii) a blast wave that is collimated in a jet (JET; Sari, Piran, & Halpern 1999; note that the evolution in the case of a jet is rather insensitive to the density structure of the ambient medium; for details see Kumar & Panaitescu 2000). The three cases have in common that the synchrotron parameters all evolve as power laws in time (i.e., $F_m = C_F t^{-\alpha_F}$, $\nu_a = C_a t^{-\alpha_a}$, $\nu_m = C_m t^{-\alpha_m}$, and $\nu_c = C_c t^{-\alpha_c}$) but differ in the values of their decay indices and coefficients. In addition to assuming model-dependent decay indices, in this paper and in Paper I we solved for α_F, α_a, α_m, and α_c explicitly by model fitting the above synchrotron spectrum (FREE). The advantage of this approach is that it assumes only that the afterglow is due to synchrotron emission with a power-law distribution of electron energies, and it imposes no physical constraints on the geometry of the outflow, the microphysics of the shock or the density structure of the circumburst medium.

3.3. *Modeling the Light Curves*

We fit the function $F(\nu, C_F, C_a, C_m, C_c, \alpha_F, \alpha_a, \alpha_m, \alpha_c, p)$ in equation (3) to the observations presented in Paper I, this work (Tables 1 and 2) and the early time optical data of Castro-Tirado et al. (2001). We minimize the χ^2 of the fit by the Levenberg-Marquardt least-squares minimization scheme. We account for the effect of interstellar scintillation by adding in quadrature the predicted scatter due to ISS (see previous discussion) to the measurement error. We determine the 68.3% (1 σ) uncertainties in the parameters by plotting contours in chi-squared where χ^2 is raised by 2.3 as a function of the two relevant parameters and by leaving the remaining parameters free. The result of the best fits are shown in Figure 1 and presented in Table 3.

In addition to this free-form model (FREE), we also fixed the decay rate parameters (α_F, α_a, α_m, and α_c) at the predicted values for the constant density ISM, the WIND, and the JET model and repeated the fit. The results of the JET fit are shown in Figure 3 and presented in Table 3. As expected from the earlier attempts in Paper I, the standard WIND and constant density ISM fits were rejected as unsuitable ($\chi^2_r > 8$). These fits do not account well for the combination of the rapid decay at optical wavelengths and the more shallow decay at radio wavelengths.

4. DISCUSSION

The principal challenge in modeling the afterglow of GRB 991208 is in simultaneously fitting for the decay of the radio ($\alpha_R = 1.07 \pm 0.09$) and optical ($\alpha_o = 2.2 \pm 0.1$) light curves. The model that best represents the data is the free-form model (FREE) in which all the parameters in equation

TABLE 3
BEST FIT MODEL PARAMETERS FOR GRB 991208

p	C_F (mJy)	C_a (GHz)	C_m (THz)	C_c (THz)	α_F	α_a	α_m	α_c	χ^2_r	dof	Note
$2.14^{0.16}_{-0.09}$	$7.7^{15.7}_{-2.3}$	28^{72}_{-12}	$0.34^{0.29}_{-0.30}$	2670^{1200}_{-600}	$0.34^{0.28}_{-0.74}$	$0.29^{0.21}_{-0.17}$	$1.9^{1.8}_{-1.2}$	$2.08^{0.20}_{-0.11}$	1.52	104	FREE
$2.36^{0.19}_{-0.03}$	$17.8^{4.2}_{-1.2}$	$6.3^{2.0}_{-1.9}$	$39.4^{60.1}_{-3.10}$	$3.0^{1.8}_{-2.1}$	1.0	0.2	2.0	0.0	1.89	108	JET

NOTES.—The value of p, the peak flux density $F_m = C_F \times t_d^{-\alpha_F}$, the synchrotron self-absorption frequency $\nu_a = C_a \times t_d^{-\alpha_a}$, the peak frequency $\nu_m = C_m \times t_d^{-\alpha_m}$, the cooling frequency $\nu_c = C_c \times t_d^{-\alpha_c}$, the reduced chi-squared χ^2_r, and the degrees of freedom (dof) of the fit. Fixed parameters can be recognized by the fact that they have no quoted uncertainties.

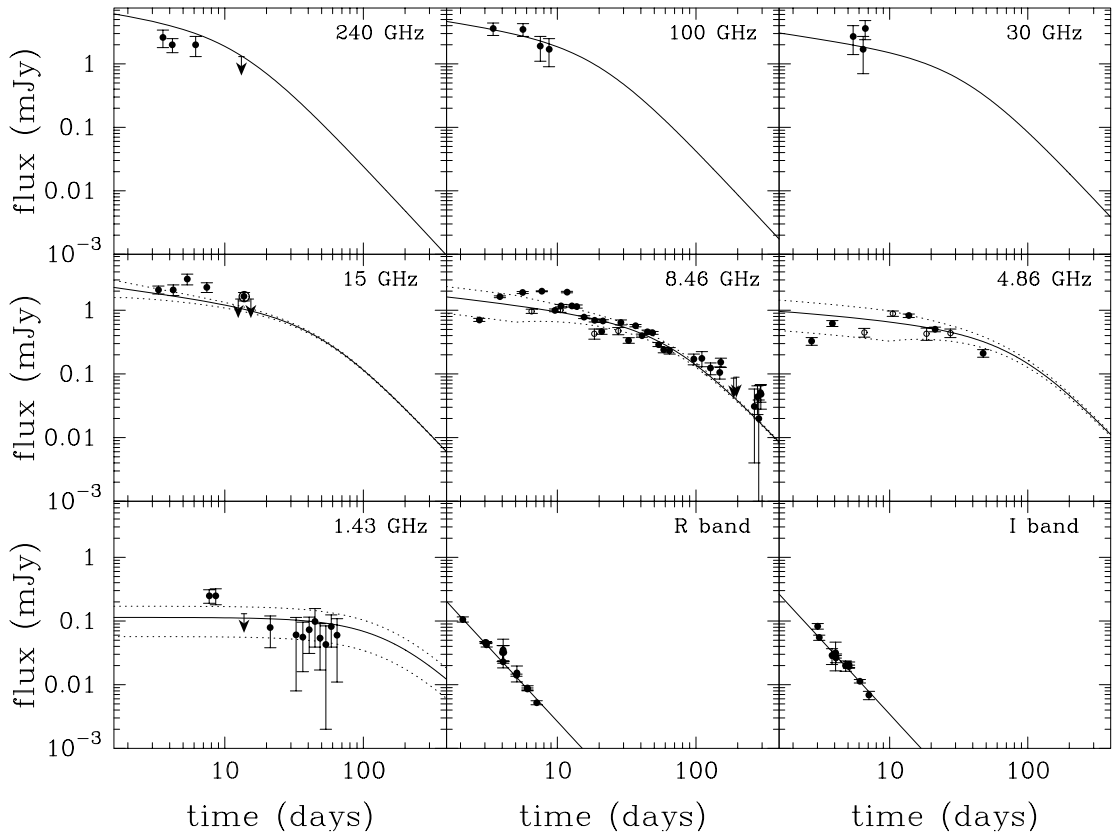

FIG. 3.—Radio to optical light curves of GRB 991208. The solid line indicates the best fit to the light curves for the JET model, and the dotted lines are the predicted rms scatter due to interstellar scintillation. See § 3 for more details.

(3) were solved for. The FREE model shown in Figure 1 and summarized in Table 3 differs from the original model presented in Paper I in several respects. Most notably, with the addition of the optical data from Castro-Tirado et al. (2001), it has been necessary to allow for a cooling break between the optical and millimeter bands (§ 3.2). This has the effect of flattening the value of p which improves the fit to the decay of the optical light curve. A cooling break in the spectrum also alters the temporal decline of the synchrotron parameters, but the values in Table 3 agree, within the errors, to those derived in Paper I. The FREE model resolves the differences between α_R and α_o by allowing for a relatively shallow decay of the peak flux density, i.e., $F_m \propto t^{-0.34}$, and an unusually rapid evolution of the cooling frequency to lower frequencies, i.e., $\nu_c \propto t^{-2.1}$. This is generally much faster than any model yet proposed for GRB afterglows. For $\nu_c \propto t^{-2}$ this implies $\Gamma \times B^3 = \text{constant}$ (where Γ is the bulk Lorentz factor of the flow and B is the postshock magnetic field). For any reasonable model both Γ and B are *decreasing* with time unless either the circumburst density or the fraction of shock energy in the B-field ϵ_B is increasing in time. In a future paper (S. Yost et al. 2003, in preparation) we plan to explore such modifications to the standard model for a number of well-studied afterglows.

Both Li & Chevalier (2001) and Panaitescu & Kumar (2002) suggested a revision to the basic afterglow model in order to overcome the difficulties with jointly fitting the radio and optical data for this burst. They proposed the existence of a two-component electron energy distribution with different slopes above and below some break frequency ν_b. Reasonable fits were obtained for either WIND and JET models provided that the radio (optical) emission was dominated by the low (high) energy electrons. Li & Chevalier (2001) also made predictions for the future evolution of the afterglow beyond the first two weeks, allowing further tests of their model. The measured $\alpha_R \sim 1.1$ for the 8.46 GHz light curve is in good agreement with their predicted decay $\alpha_R = 1.25$. The largest source of disagreement is in the low-frequency behavior. In their WIND model the peak flux density at 1.43 GHz is predicted to be a factor of 10 times larger than what is measured. This is likely due to the relatively slow evolution of ν_a where $\alpha_a = 0.29$, a value that is closer to the JET model ($\alpha_a = 0.2$) than the WIND model ($\alpha_a = 0.6$).

In Paper I when the spectral fits were compared with the expectations for specific models, satisfactory agreement was found for the JET model. Nevertheless, there were a number of discrepancies, notably the decline in the peak flux density F_m was too shallow, and the value for the slope of the electron energy distribution $p = 2.52$ was steeper than that implied by the decay of the optical light curves $p \sim 2.2$. It was proposed that these problems with the JET model could be reconciled if the jet was in transition to its fully asymptotic behavior. In our new JET model (see Fig. 3 and Table 3), the addition of a cooling break improves the overall quality of the fit considerably. Despite this agreement, there is a suggestion in Fig. 3 that the JET model is having some difficulties with the late-time radio measurements. Most of the excess χ^2 in the JET model results from the fact that the late-time light curve ($\Delta t > 100$ days) at 8.46 GHz is flat, $\alpha_R \sim 1.1$, whereas the JET model predicts that the flux density will fall as $F_\nu \propto t^{-p}$, in agreement with $\alpha_o \sim 2.2$.

There are two additional effects, not accounted for in our analysis, that could make $\alpha_R < \alpha_o$. In the first instance, GRB 991208 could have occurred in a radio-bright host galaxy (e.g., Berger, Kulkarni, & Frail 2001). Sokolov et al. (2001) have used various optical methods to estimate the star formation rate (SFR) for the host galaxy of GRB 991208 and derive an extinction-corrected SFR $\gtrsim 100\ M_\odot\ \mathrm{yr}^{-1}$. Although there are large uncertainties in such estimates, at $z = 0.7$ such elevated SFRs should be detectable at centimeter wavelengths. Assuming a standard starburst spectral energy distribution (Yun & Carilli 2002), we predict $F_\nu(1.43\ \mathrm{GHz}) \approx 110\ \mu\mathrm{Jy}$, significantly brighter than our measurements. We can therefore infer that the SFR in the host of GRB 991208 is probably no higher than a few tens of $M_\odot\ \mathrm{yr}^{-1}$. Deeper radio observations taken a year or more after the burst, when the emission from the afterglow is negligible, are needed to provide a more accurate estimate of the star formation rate. Another possible source of the flattening of the radio light curves could be the transition of the relativistic blast wave to nonrelativistic expansion. Frail, Waxman, & Kulkarni (2000) modeled the decay of the radio light curves for GRB 970508 at $\Delta t \gtrsim 100$ days as a nonrelativistic expansion. The expected decay rate in this phase of the evolution is $\alpha_{\mathrm{NR}} = 3(p-1)/2 - 3/5 \approx 1.2$ for $p = 2.2$. Thus, it is possible that the difference in decay rates is due to a transition to nonrelativistic expansion at $t \sim 40$ days. More sophisticated modeling is needed which explicitly includes the evolving dynamics of the blastwave (e.g., Harrison et al. 2001; Panaitescu & Kumar 2002) in order to test this hypothesis.

In summary, with continued monitoring of the bright afterglow of GRB 991208, it has been possible to track the evolution of its radio light curve out to nearly 300 days after the burst. The power-law decline of the optical light curve at early times is considerably steeper than that of the radio light curve at late times. There are several different explanations for reconciling this disparate behavior, including modifying the standard relativistic model with nonstandard electron distributions, and with circumburst densities or equipartition parameters ϵ_B that increase with time. However, the simplest explanation consistent with the data and requires no significant modifications is that the blastwave of GRB 991208 entered a nonrelativistic expansion phase several months after the burst.

APPENDIX

OBSERVED ANGULAR SIZE

The relation between observed time, T, real time t, the radius R and the angle $\mu = \cos\theta$ is given by

$$T = t - \mu R/c\ . \tag{A1}$$

R and t are related by some hydrodynamic solution given by the dynamics of the shock, so that in a given observed time T, R is a function of μ only. Shock dynamics are usually described by a power law, $\gamma \sim R^{-m/2}$. Therefore,

$$t = \frac{R}{c}\left[1 + \frac{1}{4(m+1)\gamma^2}\right]\ .$$

Substituting into equation (A1) gives

$$cT/R = 1 - \mu + \frac{1}{4(m+1)\gamma^2}\ .$$

Following Sari (1998) we define γ_L to be the Lorentz factor of the fluid behind the shock on the line of sight and R_L to be the shock radius on the line of sight, both at time T. We get

$$cT = \frac{R_L}{4(m+1)\gamma_L^2}\ . \tag{A2}$$

Substituting this in the previous expression, we have

$$1 = \frac{R}{R_L}4(m+1)\gamma_L^2\left[1 - \mu + \frac{1}{4(m+1)\gamma_L^2}\left(\frac{R}{R_L}\right)^m\right]\ ,$$

which can be rewritten as

$$1 - \mu = \frac{1}{4(m+1)\gamma_L^2}\left[\left(\frac{R}{R_L}\right)^{-1} - \left(\frac{R}{R_L}\right)^m\right]\ .$$

The perpendicular size, in which we are interested, is given by

$$R_\perp = R\sin\theta = R\sqrt{1-\mu^2} \cong \sqrt{2}R\sqrt{1-\mu}\ .$$

It is therefore maximal when $R^2(1-\mu)$ is maximal:

$$R^2(1-\mu) \propto \left(\frac{R}{R_L}\right) - \left(\frac{R}{R_L}\right)^{m+2}\ ,$$

and the maximum is obtained for

$$\frac{R}{R_L} = \left(\frac{1}{m+2}\right)^{1/(m+1)} .$$

The maximal perpendicular size from which radiation arrives is therefore given by

$$R_\perp = \sqrt{2}R\sqrt{1-\mu} = \sqrt{2}\frac{R_L}{\gamma_L}\left(\frac{R}{R_L}\right)\sqrt{\frac{1}{4(m+1)}\left[\left(\frac{R}{R_L}\right)^{-1} - \left(\frac{R}{R_L}\right)^{m}\right]}$$
$$= \frac{R_L/\gamma_L}{\sqrt{2(m+2)}}\left(\frac{1}{m+2}\right)^{1/2(m+1)} .$$

We now only need to get the coefficient for the relation between R_L and T to get a closed expression. Roughly this is given by $E \sim R^3\rho c^2\gamma^2$, where ρ is the density just in front of the shock. The more exact result is given by Blandford & McKee (1976, their eq. [69]) as

$$E = \frac{16\pi}{5+4m}R^3\rho c^2\gamma^2 . \tag{A3}$$

If we write $\rho = AR^{m-3}$, this, together with equation (A2), translates to

$$E = \frac{16\pi A}{5+4m}R_L^m c^2\frac{R_L}{4(m+1)cT} \Longrightarrow R_L = \left[\frac{(5+4m)(m+1)TE}{4\pi cA}\right]^{1/(m+1)} ,$$

$$R_L/\gamma_L = 2\sqrt{(m+1)cT}\left[\frac{(5+4m)(m+1)TE}{4\pi cA}\right]^{1/2(m+1)} .$$

Therefore,

$$R_{\perp,\max} = \sqrt{\frac{2(m+1)cT}{m+2}}\left[\frac{(5+4m)(m+1)TE}{4\pi cA(m+2)}\right]^{1/2(m+1)} .$$

For a wind we have $m = 1$, so

$$R_{\perp,\max,\mathrm{WIND}} = \sqrt{\frac{4cT}{3}}\left[\frac{3TE}{2\pi cA}\right]^{1/4} = 1.1\times 10^{17}\mathrm{cm}\left(\frac{1+z}{2}\right)^{-3/4}E_{52}^{1/4}A_*^{-1/4}(T/15\ \mathrm{days})^{3/4} ,$$

where $E = 10^{52}E_{52}$, we have corrected for redshift z and have used $A = 5\times 10^{11}A_*$ g cm^{-1} as in Chevalier & Li (2000). Or in angular size

$$\theta_{\mathrm{WIND}} = 2.2\ \mu\mathrm{as}\left(\frac{1+z}{2}\right)^{-3/4}D_{A,28}^{-1}E_{52}^{1/4}A_*^{-1/4}(T/15\ \mathrm{days})^{3/4} ,$$

where $D_{A,28}$ is the angular distance in units of 10^{28} cm. For ISM models we have $m = 3$, and

$$\theta_{\mathrm{ISM}} = 2.8\ \mu\mathrm{as}\left(\frac{1+z}{2}\right)^{-5/8}D_{A,28}^{-1}E_{52}^{1/8}n_1^{-1/8}(T/15\ \mathrm{days})^{5/8} ,$$

where n_1 is the density of the ISM in particles cm^{-3}. We can now obtain an estimate of the angular diameter for a jet as follows. During sideways expansion of the jet, the radius R of the fireball is practically constant, $\gamma \propto t^{-1/2}$ (Sari, Piran, & Halpern 1999) and so $R_{\perp,\max,\mathrm{JET}} \propto t^{1/2}$. At the time of the jet break t_{JET} we thus roughly have $R_{\perp,\max,\mathrm{JET}} = R_{\perp,\max,\mathrm{ISM}}(t_{\mathrm{JET}})\times(t/t_{\mathrm{JET}})^{1/2}$, i.e.,

$$\theta_{\mathrm{JET}} = 1.7\mu\mathrm{as}\left(\frac{1+z}{2}\right)^{-5/8}D_{A,28}^{-1}E_{52}^{1/8}n_1^{-1/8}(t_{\mathrm{JET}}/8\ \mathrm{hr})^{1/8}(T/15\ \mathrm{days})^{1/2} .$$

REFERENCES

Berger, E., Kulkarni, S., & Frail, D. A. 2001, ApJ, 560, 652
Blandford, R. D., & McKee, C. F. 1976, Phys. Fluids, 19, 1130
Castro-Tirado, A., et al. 1999, GCN Circ. 452 (http://gcn.gsfc.nasa.gov/gcn/gcn3/452.gcn3)
———. 2001, A&A, 370, 398
Chevalier, R. A., & Li, Z.-Y. 1999, ApJ, 520, L29
———. 2000, ApJ, 536, 195
Dai, Z. G., & Gou, L. J. 2001, ApJ, 552, 72
Djorgovski, S. G., et al. 1999, GCN Circ. 481 (http://gcn.gsfc.nasa.gov/gcn/gcn3/481.gcn3)
Dodonov, S., et al. 1999, GCN Circ. 475 (http://gcn.gsfc.nasa.gov/gcn/gcn3/475.gcn3)
Frail, D., et al. 1999, GCN Circ. 451 (http://gcn.gsfc.nasa.gov/gcn/gcn3/451.gcn3)

Frail, D. A., Kulkarni, S. R., Nicastro, S. R., Feroci, M., & Taylor, G. B. 1997, Nature, 389, 261
Frail, D. A., Waxman, E., & Kulkarni, S. R. 2000, ApJ, 537, 191
Galama, T. J., et al. 2000, ApJ, 541, L45
Goodman, J. 1997, NewA, 2(5), 449
Granot, J., Piran, T., & Sari, R. 1999a, ApJ, 513, 679
———. 1999b, ApJ, 527, 236
Granot, J., & Sari, R. 2002, ApJ, 568, 820
Harrison, F. A., et al. 2001, ApJ, 559, 123
Hurley, K., et al. 2000, ApJ, 534, L23
Kumar, P., & Panaitescu, A. 2000, ApJ, 541, L9
Li, Z., & Chevalier, R. A. 2001, ApJ, 551, 940
Panaitescu, A., & Kumar, P. 2002, ApJ, 571, 779
Piran, T. 2000, Phys. Rep., 333, 529
Reynolds, R. J. 1989, ApJ, 339, L29
Rickett, B. J. 1990, ARA&A, 28, 561
Sagar, R., Mohan, V., Pandey, A. K., Pandey, S. B., & Castro-Tirado, A. J. 2000, Bull. Astron. Soc. India, 28, 15
Sari, R. 1998, ApJ, 494, L49
Sari, R., Piran, T., & Halpern, J. P. 1999, ApJ, 519, L17
Sari, R., Piran, T., & Narayan, R. 1998, ApJ, 497, L17
Shepherd, D. S., et al. 1999, GCN Circ. 455 (http://gcn.gsfc.nasa.gov/gcn/gcn3/455.gcn3)
Sokolov, V. V., et al. 2001, A&A, 372, 438
Taylor, J. H., & Cordes, J. M. 1993, ApJ, 411, 674
van Paradijs, J., Kouveliotou, C., & Wijers, R. A. M. J. 2000, ARA&A, 38, 379
Walker, M. A. 1998, MNRAS, 294, 307
Yun, M. S., & Carilli, C. L. 2002, ApJ, 568, 88